remote sensing

MDPI

Article

Circum-Arctic Changes in the Flow of Glaciers and Ice Caps from Satellite SAR Data between the 1990s and 2017

Tazio Strozzi [1,*], Frank Paul [2], Andreas Wiesmann [1], Thomas Schellenberger [3] and Andreas Kääb [3]

1 Gamma Remote Sensing, 3073 Gümligen, Switzerland; wiesmann@gamma-rs.ch
2 Department of Geography, University of Zurich, 8057 Zürich, Switzerland; frank.paul@geo.uzh.ch
3 Department of Geosciences, University of Oslo, 0316 Oslo, Norway; thomas.schellenberger@geo.uio.no (T.S.); kaeaeb@geo.uio.no (A.K.)
* Correspondence: strozzi@gamma-rs.ch; Tel.: +41-31-951-7005

Received: 3 August 2017; Accepted: 8 September 2017; Published: 12 September 2017

Abstract: We computed circum-Arctic surface velocity maps of glaciers and ice caps over the Canadian Arctic, Svalbard and the Russian Arctic for at least two times between the 1990s and 2017 using satellite SAR data. Our analyses are mainly performed with offset-tracking of ALOS-1 PALSAR-1 (2007–2011) and Sentinel-1 (2015–2017) data. In certain cases JERS-1 SAR (1994–1998), TerraSAR-X (2008–2012), Radarsat-2 (2009–2016) and ALOS-2 PALSAR-2 (2015–2016) data were used to fill-in spatial or temporal gaps. Validation of the latest Sentinel-1 results was accomplished by means of SAR data at higher spatial resolution (Radarsat-2 Wide Ultra Fine) and ground-based measurements. In general, we observe a deceleration of flow velocities for the major tidewater glaciers in the Canadian Arctic and an increase in frontal velocity along with a retreat of frontal positions over Svalbard and the Russian Arctic. However, all regions have strong accelerations for selected glaciers. The latter developments can be well traced based on the very high temporal sampling of Sentinel-1 acquisitions since 2015, revealing new insights in glacier dynamics. For example, surges on Spitsbergen (e.g., Negribreen, Nathorsbreen, Penckbreen and Strongbreen) have a different characteristic and timing than those over Eastern Austfonna and Edgeoya (e.g., Basin 3, Basin 2 and Stonebreen). Events similar to those ongoing on Eastern Austofonna were also observed over the Vavilov Ice Cap on Severnaya Zemlya and possibly Simony Glacier on Franz-Josef Land. Collectively, there seems to be a recently increasing number of glaciers with frontal destabilization over Eastern Svalbard and the Russian Arctic compared to the 1990s.

Keywords: Arctic; glaciers; ice caps; flow; surge; PALSAR-1; Sentinel-1

1. Introduction

Glaciers and ice caps (GIC) on Arctic islands (excluding those on Greenland and Iceland) contribute significantly to sea level rise even if they cover only nearly one third of the total glacier area [1]. According to [2] the sea level equivalent of the collective Arctic GIC mass is about 16 cm or 40% of all glaciers worldwide. At the same time, past and potential future temperature increase in the Arctic is higher than elsewhere on Earth due to pronounced albedo feedbacks from the vanishing sea ice (the so-called Arctic amplification, e.g., [3]). Higher temperatures and a reduction in sea ice cover can have an array of effects, for example a change in the thermal regime of the ice, an increase in precipitation with positive mass budgets and advancing glaciers, direct ocean-glacier interactions such as reduction of buttressing by sea ice or inflow of ocean warm water to calving fronts, or a higher equilibrium line that potentially turns the entire ice cap into an ablation zone. If the latter occurs too often, the highest point of the ice cap might reach an elevation from where it is impossible to recover (e.g., [4]). In case a mass gain by

increased precipitation can compensate the mass loss from increased temperatures, the total glacier mass will not change necessarily. However, the climatic regime of an affected glacier becomes more maritime (warm/wet), potentially resulting in an acceleration of glacier flow and maybe also in a change of its thermal regime. Higher flow velocities will also increase friction at the glacier bed, generating energy to melt basal ice, lubricate the flow, and through enhanced straining and associated crevassing facilitate ingress of surface meltwater, thus forming a positive feedback process to accelerate ice flow [5]. Faster flow means higher mass flux and, for the large number of tidewater glaciers in the Arctic, also an increase in calving flux and thus contribution to sea level rise (for land-terminating glaciers the tongues will advance without impacting on sea level). The calving flux of a glacier can be determined by multiplying its flow velocity with its cross section at its grounding line [6]. Whereas the cross sections are often not well known and have to be derived from modelling (e.g., [7]) or some rough assumptions [8], surface flow velocities can be accurately determined from satellite data. For calving glaciers, variations in flow velocities are directly related to the ice mass flux and an assessment of long-term trends and/or seasonal variations from satellite data would improve the related estimates.

By reason of the large potential contribution of Arctic GIC to sea level and the already observed increased mass loss for some of the Arctic islands (e.g., [9,10]) several studies have recently investigated flow velocities, changes in velocity, and also elevation changes from altimetry for numerous Arctic GIC in great detail. For example, over the Canadian Arctic [11] analysed velocities of the Devon Ice Cap, Van Wychen, W. et al. [12] presented flow velocities and discharge for all of the glaciers and ice caps on Baffin and Bylot islands, and Van Wychen, W. et al. [13] studied multi-temporal trends in velocity and discharge for Ellesmere and Axel Heiberg Islands. This region was also investigated by [8] with a focus on mass budgets (both surface and calving) for the 1991–2015 period. Similarly, Melkonian, A. et al. [14] investigated velocities and elevation changes for Novaya Zemlya (Russian Arctic) and numerous studies have analysed the changes in Svalbard (e.g., [5,15,16]) with a special focus on surge-type (e.g., [17–19]) or continuously fast-flowing (e.g., [20]) glaciers. However, there are no comprehensive recent studies on flow velocities for GIC on Franz Josef Land and Severnaja Zemlya, only older ones [21,22] or short communications on rapid glaciers changes [23].

All recent studies benefit from the largely automated processing of image-pairs using offset-tracking (e.g., [24,25]) that can thus be applied to large regions using both optical (e.g., [26,27]) and SAR sensors [28,29]. Whereas SAR sensors have so far mainly been used to obtain short-term fluctuations and trends in surface velocity for glaciers in polar regions, optical data have been used to obtain decadal trends also in sub-polar and mid-latitude regions [30]. However, the high spatial resolution and repeat interval of optical satellites such as Sentinel 2A/B now also allow investigation of flow velocities on a weekly temporal scale [31,32] and the former temporal distinction has become less clear in this regard. With the increasing overlap of scenes towards the poles, very short observation periods become possible, at least as long as clouds, polar night and shadow (for optical) and the acquisition plans (for SAR) permit. Still, the short-term glacier flow variability accessible to date through satellites provides new insights in glacier dynamics and the governing processes, whereas the long-term trends better reflect variations in mass balance and changes in flow regimes, thus direct or indirect impacts of climate change.

The current rapid increase of archived and newly acquired optical and SAR satellite data in the Arctic that are available for quantifying glacier surface flow, together with progress in methods for handling large satellite data sets, open up new possibilities to monitor ice flow over large regions and to detect and understand related changes. In this study, we:

- demonstrate the use of automated processing lines to obtain velocity fields from SAR sensors over large Arctic regions for at least two points in time over the last 20 years;
- assess the accuracy of Sentinel-1 for relatively small Arctic glaciers detect long-term changes across regions and identify glaciers where dramatic changes are taking place;
- utilize the dense temporal coverage of Sentinel-1 in order to obtain velocity time-series for selected rapidly changing (e.g., surging) glaciers;

- better understand the dynamic behaviour of glacier instabilities.

Overall, this study should provide an overview of the flow velocities, their long-term changes and selected short-term fluctuations for Arctic glaciers. It is, however, not the focus of this work to discuss glaciological details of all individual sites.

2. Sites, Data and Methods

2.1. Study Regions

In order to efficiently use the resources available to us for the present study and at the same time still cover a wide climatic and geographic range of regions, we focus our investigations on the GIC of the Canadian Arctic North and South, Svalbard and the Russian Arctic (Figure 1), excluding Greenland GIC where the related data analysis is still ongoing.

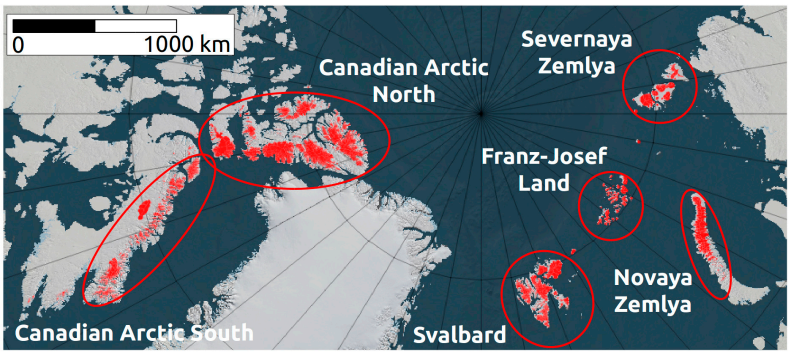

Figure 1. Study regions with glacierized areas (in red) according to RGI 5.0 [33].

The Canadian Arctic archipelago is situated in the northern extremity of North America between 65° and 83°N and extends some 2400 km longitudinally and 1900 km latitudinally. Glaciers and ice caps are occupying in particular the major islands to the east, which are mountainous with peaks over 2000 m a.s.l. According to the Randolph Glacier Inventory (RGI) 5.0 [33] the glacierized areas around the year 2000 were 105,000 km^2 over the Canadian Arctic North and 40,888 km^2 over the Canadian Arctic South, making the Canadian Arctic the largest glacierized region outside of the ice sheets. The distribution of glaciers consists of large outlet glaciers extending from the high elevation ice cap interior to the margins, separate remnant ice masses that have become detached from the ice cap proper, and isolated ice patches in low-lying areas [12,13].

The average annual temperature may be as low as −20 °C in the north and −6 °C in south, with extreme low temperatures in the order of −50 °C [34]. In the High Arctic islands, summer temperatures may rise above freezing for only one or two months. Annual precipitation is low, ranging from 400 mm in the south to less than 100 mm in the centre. Because there is generally low interannual variability in precipitation and high variability in melt production, interannual variability in the regional surface mass budget is largely governed by changes in the summer surface air temperatures [10]. Since the late 1980s, and especially since 2005, changing summer atmospheric circulation patterns have increased advection of warm air from the north-west Atlantic to the Canadian High Arctic, leading to increased surface melt and longer melt seasons. As a consequence, ice loss via surface mass balance has increased sharply in recent years [10].

The Svalbard archipelago is situated between 74° and 81°N. The total area of the archipelago is about 62,000 km^2, of which 37,705 km^2 correspond to Spitsbergen, the largest island. According to RGI 5.0, 1668 glaciers covered 33,837 km^2 (57% of the landmass) in the late 2000s. The geometry of the glacierized areas is complex and several types of glaciers are found. Valley glaciers in the mountains and tidewaters glaciers along the coastline are commonly found, but there are also ice caps divided in various basins, in particular over eastern Spitsbergen, Edgeøya, Barentsøya, and Nordaustlandet. During the past century,

most glaciers in Svalbard have been in retreat from their maximum extent during the Little Ice Age [6]. Surge-type glaciers are very common in Svalbard [35].

The climate of Svalbard is the result of its high latitude and the strong influence of the warm ocean water from the North Atlantic Current, which makes the climatic conditions much milder than expected for such latitudes. The temperature varies significantly across the archipelago with the northern parts of Spitsbergen about 5 °C colder in winter than the south and only 3 °C in summer [36]. On average, the coldest temperatures are between −20 °C and −13 °C and the warmest between 3 °C and 7 °C. Precipitation also shows a large spatial variability across the archipelago, with a clear gradient from west to east, ranging from values as low as 190 mm/year to reach 1200 mm/year [37]. The temperature started to increase gradually at the end of the 20th century and beginning of 21st, experiencing the greatest temperature rise in Europe during the last three decades [38].

The Russian Arctic encompasses the three Archipelagos of Novaya Zemlya, Franz-Josef Land and Severnaya Zemlya. Novaya Zemlya lies north of the Russian mainland, between the Barents and Kara Seas. The two islands of Novaya Zemlya stretch from about 70° to 77°N. Small valleys and mountain glaciers dominate the southern Island and are also present up to 74.1°N on the northern island. Further north two stronger glacierized mountain ranges and a large main ice cap, as the most prominent feature of Novaya Zemlya with a length of about 400 km, are present [39]. Whereas most of the glaciers that are separated from the main ice cap are land terminating, the large outlet glaciers of the main ice cap are mostly marine terminating [14,40]. Several glaciers on Novaya Zemlya have been identified as surge type [41]. The Franz-Josef Land archipelago is situated between 79°5′ and 82°0′ north within the Arctic Ocean, 360 km north of Novaya Zemlya and 260 km east of Svalbard. Eighty-five percent of the archipelago is covered by glaciers and ice caps distributed over many islands. The Severnaya Zemlya archipelago separates the two marginal seas of the Arctic Ocean, the Kara Sea in the west and the Laptev Sea in the east, and is situated between 78° and 81° N. Glaciers over Severnaya Zemlya have a characteristic dome shape with a continuously decreasing surface towards their edges. Approximately 50% of the 36,800 km^2 archipelago of Severnaya Zemlya is ice covered [21]. According to RGI 5.0 the glacierized areas around 2000–2010 over Severnaya Zemlya were 16,701 km^2. Over Novaya Zemlya and Franz Josef Land the glacierized areas according to RGI 5.0 were 22,128 km^2 and 12,762 km^2, respectively.

The climate in Novaya Zemlya is influenced by the North Atlantic-derived water of the Barents Sea, where the island provides an orographic barrier for eastwards moving Atlantic cyclonic systems. The warmest and wettest conditions are found in the south-west (~−5 °C and ~400 m/year, respectively) and become colder (~−10 °C) and dryer (~300 mm/year) to the north-east [42]. Precipitation is subjected to a large seasonal and interannual variation with peak precipitation rates in August and driest in April. The main forces influencing the climate of Franz Josef Land are the heavy glacier cover and sea ice. At 81° north the archipelago experiences more than 100 days of polar night and more than 100 days of midnight sun. Even during summer the angle of the sun ray spreads the limited radiated energy over a large area. Further cooling is caused by the high amount of cloudiness [43]. Average annual precipitation at the coastal stations of Franz Josef Land is between 100 and 150 mm, with the wettest months being from July through September [44]. Elevated areas can experience considerably higher precipitation. Mean annual temperatures in Severnaya Zemlya are about −16 °C, compared with about −12 °C in Franz Josef Land and −9 °C in Novaya Zemlya [43]. Severnaya Zemlya is quite dry, with average annual precipitation at the coastal stations between 220 and 270 mm and an increase in precipitation towards the summits of the major ice caps [21]. Monthly average temperature ranges from −28 °C in February to 1 °C in July.

2.2. Data

2.2.1. Satellite SAR Data

Our work is largely driven by satellite data availability. The analyses over the Canadian Arctic, Svalbard and Russian Arctic were mainly performed with ALOS-1 PALSAR-1 and Sentinel-1 data of the

time periods 2007–2011 and 2014–2017, respectively. JERS-1 SAR (1994–1998), TerraSAR-X (2008–2012), Radarsat-2 (2009–2016) and ALOS-2 PALSAR-2 (2015–2016) data were used to fill-in spatial or temporal gaps. Radarsat-2 Wide Ultra Fine (2016–2017) data were considered for validation of the Sentinel-1 results. Sensors, acquisition dates and time intervals of the SAR image pairs considered in our study over the different study regions are summarized in the Supplementary Table S1.

2.2.2. Satellite Optical Data

This study relies mostly on satellite SAR data. Landsat data available from the U.S. Geological Survey were only used to analyse recent glacier advances or retreats, and infer surge surface characteristics. We considered in particular a Landsat-4 image of 22-07-2006 and a Landsat-8 image of 27-08-2014 over Simony Glacier on McClintock Island (Franz Josef Land) and a Landsat-7 image of 07-09-2010 and a Landsat-8 image of 15-07-2016 over the Vavilov Ice Cap (Severnaya Zemlya).

2.2.3. Digital Elevation Data

Digital Elevation Models (DEM) were used for the satellite SAR data geocoding. Over the Canadian Arctic (both North and South) the digital elevation data used are from GeoBase® (http://www.geobase.ca/geobase/en/index.html). The source digital data is extracted from the hypsographic and hydrographic elements of the Canadian National Topographic Data Base (NTDB) at scale 1:250,000. The DEM is provided in 3 arcsec geographic coordinates, corresponding to a posting of approximately 90 m. Over Svalbard, Novaya Zemlya and Franz Josef Land we used the TanDEM-X Intermediate DEM (IDEM) [45]. IDEM was provided in 3 arcsec geographic coordinates with indicated absolute horizontal and vertical accuracies of less than 10 m. The IDEM is based over Svalbard on TanDEM-X acquisitions from 12 December 2010 to 26 March 2012, and over Franz Josef Land and Novaya Zemlya on TanDEM-X acquisitions from 12 December 2010 to 2 April 2011. Finally, for Severnaya Zemlya we considered the digital elevation data derived from Soviet Union topographic maps of 1:100,000 and 1:200,000 scale by Viewfinder Panoramas (http://www.viewfinderpanoramas.org), also provided in 3 arcsec geographic coordinates.

2.2.4. Glacier Outlines

Glacier outlines were used for visual representation of the ice-covered regions and are taken from RGI 5.0 [33]. Over the Arctic Canada North (RGI region 03) the glacier outlines were created from late summer, cloud free 1999–2003 Landsat 7 (ETM+) imagery and from 2002–2003 ASTER imagery. Over the Arctic Canada South (RGI region 04) the outlines were created from late-summer Landsat 7 ETM+ imagery acquired between 1999 and 2002, late-summer SPOT 5 imagery acquired between 2006–2010 and 1958 or 1982 aerial photographs. Over Svalbard (RGI region 07) the satellite images used to generate the outlines were SPOT5 5 m panchromatic stereo images from 2007–2008 (71% of the glacier area), ASTER scenes from as early as 2001 (16%), and Landsat scenes from 2000 to 2010 (less than 14%). Over the Russian Arctic (RGI region 09) the glacier outlines were digitized from orthorectified satellite imagery acquired during summers between 2000 and 2010. SPIRIT SPOT5 scenes were used for most of Novaya Zemlya, while the best available Landsat scenes were used elsewhere.

2.3. Methods

Satellite SAR images were processed with offset-tracking procedures [24,25] to three-dimensional ice surface displacement maps combining the slant-range and azimuth offsets by assuming that flow occurs parallel to the ice surface as estimated from the DEM (e.g., [46]). Matching window sizes of 64 × 196, 64 × 256, 128 × 128 and 512 × 128 pixels were applied to the ALOS-1 PALSAR-1, JERS-1 SAR, Radarsat-2 Wide Ultra-Fine (WUF) and Sentinel-1 Interferometric Wide Swath (IWS) data, respectively. The ALOS-2 PALSAR-2 ScanSAR images were multi-looked by a factor of 5 in the azimuth direction and converted to logarithmic scale before applying the offset-tracking algorithm with matching window sizes of 128 × 128 pixels. Mis-matches or blunders were filtered by applying a threshold on the correlation coefficient,

by iteratively discarding spurious matches based on the angle and size of displacement vectors in the surrounding area, and by using a low-pass filter on the resulting fields [25].

3. Results

3.1. Ice Surface Velocity Maps of Arctic Glaciers and Ice Caps

Nearly complete ice surface velocity maps for the glaciers and ice caps over the Canadian Arctic North, Canadian Arctic South and Novaya Zemlya were derived using winter ALOS-1 PALSAR-1 images of the time period 2007–2011 (Figure 2a,b,d, respectively). An ice surface velocity map for part of the Svalbard Archipelago was computed for the time period 1994–1998 using JERS-1 SAR data (Figure 2c). The JERS-1 images, available from a previous study by [22] and re-processed, only cover the eastern sector of the Svalbard Archipelago and are complemented over Edgeøya to the east with ALOS-1 PALSAR-1 data of 2010–2011 and over Kronebreen to the west with TerraSAR-X data of 2008. Unfortunately, there are no archived ALOS-1 PALSAR-1 image pairs suitable for offset-tracking over western Svalbard. Other JERS-1 data were acquired by the European Space Agency (ESA) facility in the past but are currently not distributed.

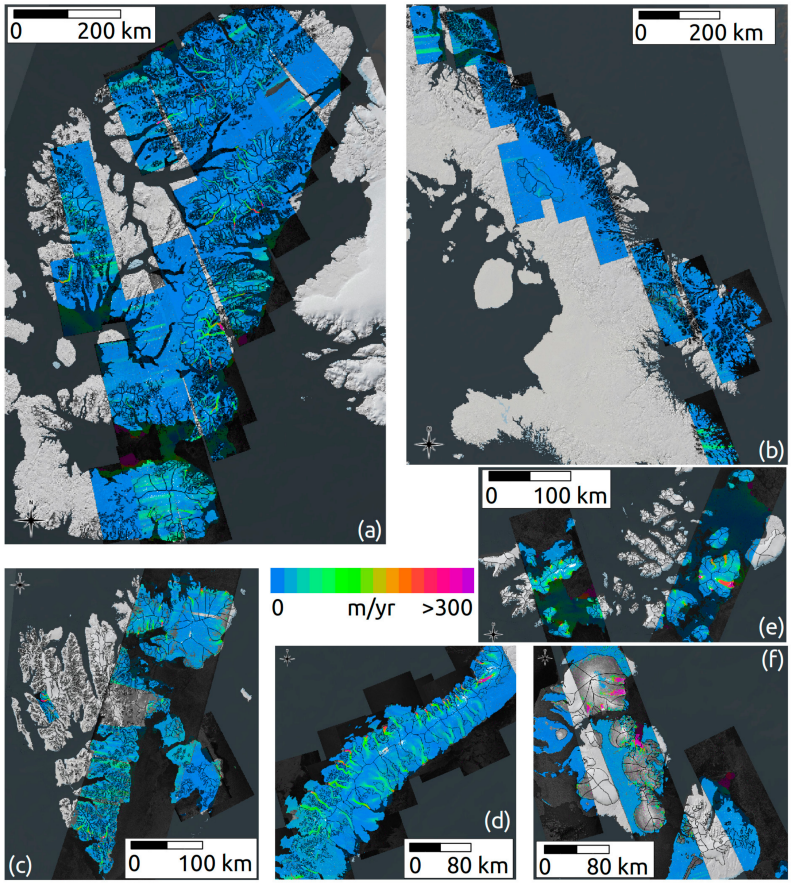

Figure 2. Ice velocity maps for (**a**) the Canadian Arctic North from ALOS-1 PALSAR-1 data of 2007 to 2011; (**b**) the Canadian Arctic South from ALOS-1 PALSAR-1 data of 2007 to 2011; (**c**) the Svalbard Archipelago from JERS-1 SAR data of 1994 to 1998 complemented by ALOS-1 PALSAR-1 data of 2010–2011 to the east and TerraSAR-X data of 2008 to the west; (**d**) Novaya Zemlya from ALOS-1 PALSAR-1 data of 2008 to 2009; (**e**) Franz-Josef Land from JERS-1 SAR data of 1998 in the east and ALOS-1 PALSAR-2 data of 2010 in the west; and (**f**) Severnaya Zemlya from ALOS-1 PALSAR-1 data of 2010. Details on the acquisition dates and time intervals of the satellite SAR data are listed in the Supplementary Table S1.

Also over Franz-Josef Land and Severnaya Zemlya there are no archived ALOS-1 PALSAR-1 image pairs suitable for large scale monitoring. Over Franz-Josef Land (Figure 2e) an ALOS-1 PALSAR-1 velocity map to the west is complemented by a JERS-1 velocity map to the east. Over Severnaya Zemlya (Figure 2f) we found in the ALOS-1 PALSAR-1 archive three image pairs acquired in 2010, but two of them are from the summer months and thus limited in their spatial coverage, in particular in the interior of the ice caps. An overview of the time periods of the ice velocity maps of Figure 2 with the indication of the employed SAR sensors is given in Table 1, while the Supplementary Table S1 reports the complete list of acquisition dates and time intervals.

The large number of Sentinel-1 images acquired since the launch of the mission in 2014 over the Canadian Arctic permits to compute complete ice surface velocity maps with high temporal sampling. In Figure 3a,b we present the ice surface velocity maps for the winter 2015 over the Canadian Arctic North and for the winter 2016 over the Canadian Arctic South, respectively. Repeated Sentinel-1 acquisitions over Svalbard were first performed during the ramp-up phase of the satellite in August 2014 at reduced resolution and twice in January and February 2015, then, since August 2015, acquisitions started on a regular 12-days basis until late 2016, when the temporal sampling was increased to 6 days after the successful launch of Sentinel-1B. In Figure 3c we present an averaged velocity map calculated from winter measurements in 2015 and 2016.

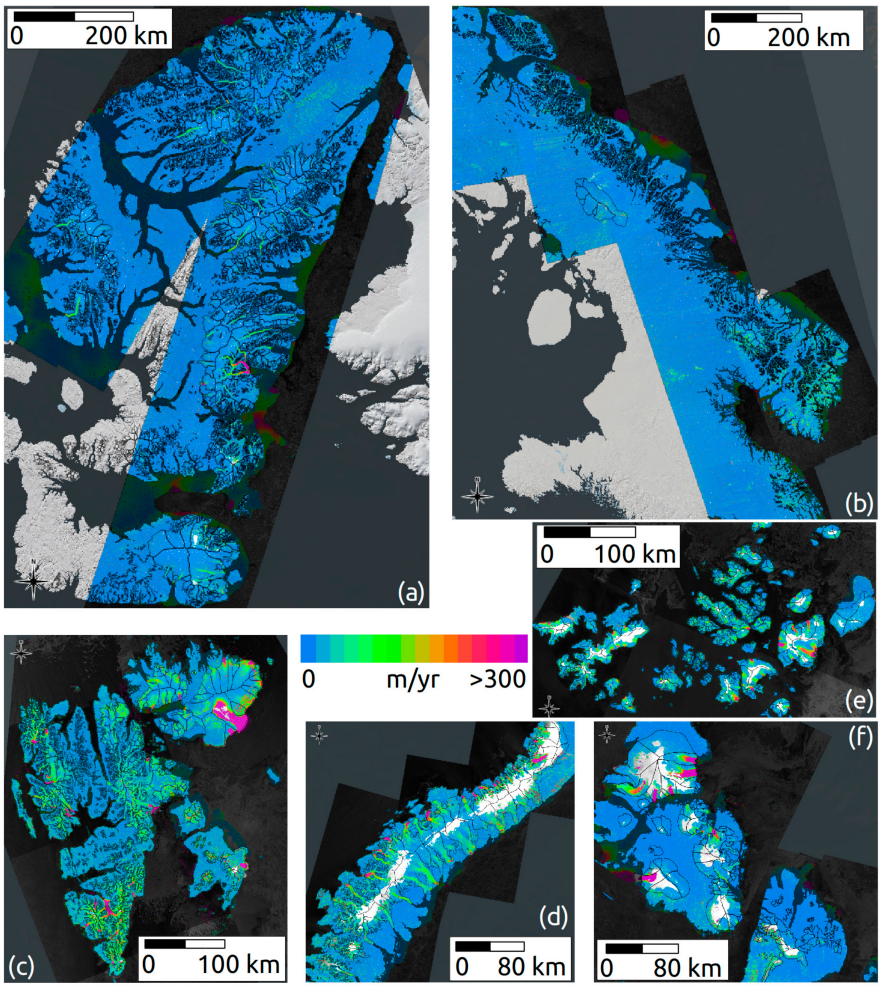

Figure 3. Ice velocity maps from Sentinel-1 SAR winter data of (**a**) 2015 over the Canadian Arctic North; (**b**) 2016 over the Canadian Arctic South; (**c**) 2015–2016 (average) over the Svalbard Archipelago; (**d**) 2017 over Novaya Zemlya; (**e**) 2016 over Franz-Josef Land; and (**f**) 2016–2017 over Severnaya Zemlya.

Over the Russian Arctic regular monitoring with Sentinel-1 data is ongoing since October 2016, when Sentinel-1B was becoming operational. In Figure 3d–f we present the results for the winter of 2016/2017 for Novaya Zemlya, Franz-Josef Land and Severnaya Zemlya, respectively. The C-band (Sentinel-1) winter velocity maps over the Russian Arctic Islands are not as complete in the interiors of the ice caps as the L-band based maps (JERS-1 SAR and ALOS-1 PALSAR-1).

Table 1. Overview of sensors and time periods for the ice velocity maps of Figures 2 and 3 for the different study regions.

Study Region	Satellite Sensor	Time Period
Canadian Arctic South	PALSAR-1 Sentinel-1	2007–2011 2015
Canadian Arctic South	PALSAR-1 Sentinel-1	2007–2011 2016
Svalbard	JERS-1/PALSAR-1/TerraSAR-X Sentinel-1	1994–2011 2015–2017
Novaya Zemlya	PALSAR-1 Sentinel-1	2008–2010 2017
Franz-Josef Land	JERS-1/PALSAR-1 Sentinel-1	1998–2011 2016
Severnaya Zemlya	PALSAR-1 Sentinel-1	2010 2016–2017

3.2. Variability of Glacier Dynamics in the Arctic Canada

In order to visualize changes in the ice surface velocity from 1994–2011 to 2015–2017, we computed difference maps between the results of Figure 2 and those of Figure 3. Over the Canadian Arctic North (Figure 4a) our ALOS-1 PALSAR-1 2007–2011 and Sentinel-1 2015 results confirm the findings of [13] using Radarsat-1/2, ALOS-1 PALSAR-1 and Landsat-8 data of the time periods 2000 and 2010–2015. Several of the major tidewater-terminating glaciers have decelerated in recent years (Figure 5a,b), while Trinity and Wykeham Glaciers in the southeast of Ellesmere Island have accelerated (Figure 5c,d). Van Wychen, W. et al. [13] observed that the resulting increase in dynamic discharge from these two glaciers entirely compensates for the decrease in discharge from the other tidewater glaciers.

Over the Canadian Arctic South we observe with both ALOS-1 PALSAR-1 winter images of the time period 2007–2011 (Figure 2b) and Sentinel-1 images of winter 2016 (Figure 3b) slow moving glaciers with velocities generally below 100 m/year. In the difference map of Figure 4b we do not spot any significant signal, apart from some ionospheric disturbances in the north-west of the study region. Because of the slow ice movements both ALOS-1 PALSAR-1 and Sentinel-1 differential winter interferograms show a high degree of coherence. Fringe images could thus support the delineation of the glacier's drainage basins [39].

3.3. Variability of Glacier Dynamics over Svalbard

By comparing velocities from the 1990s (Figure 2c) and 2015–2016 (Figure 3c) over Svalbard (Figure 4c) we recognize in particular the wide surge of Basin-3 over Austfonna in the north-east of the archipelago [5,15]. Figure 6a–c show three snapshots of the Basin-3 surge on JERS-1 SAR data of 1998, ALOS-1 PALSAR-1 data of 2010 and Sentinel-1 data of 2016. Further inspection of the difference map of Figure 4c indicates that frontal destabilisation processes are ongoing also on the basin south of Basin-3, called Basin-2 North in [19], and on Stonebreen on Edgeøya, the large island south of Austfonna [18]. In addition, the close-up of the ice surface velocity map for the 26th of June to the 7th of August 2016 (Figure 6c) indicates that on Basin-2 there is also another flow unit that was active in the summer of 2016.

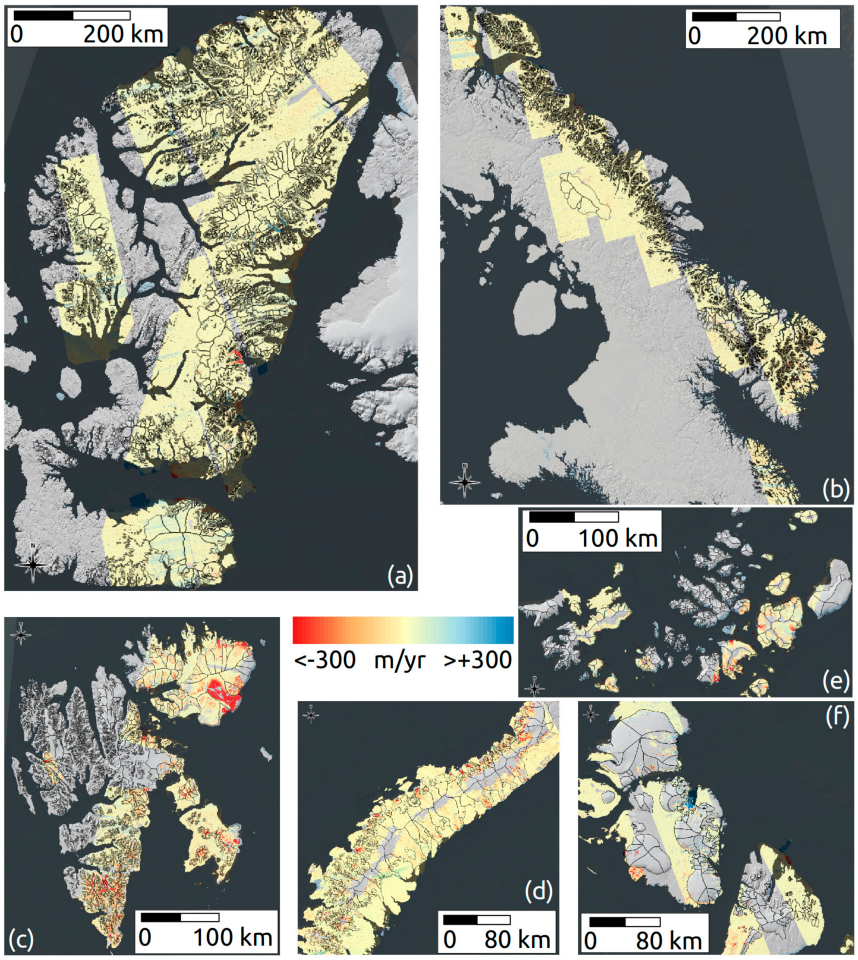

Figure 4. Difference map of the ice velocity results of Figure 2 (1994–2011) and 3 (2015–2017). (**a**) the Canadian Arctic North, (**b**) the Canadian Arctic South, (**c**) the Svalbard Archipelago, (**d**) Novaya Zemlya, (**e**) Franz-Josef Land and (**f**) Severnaya Zemlya.

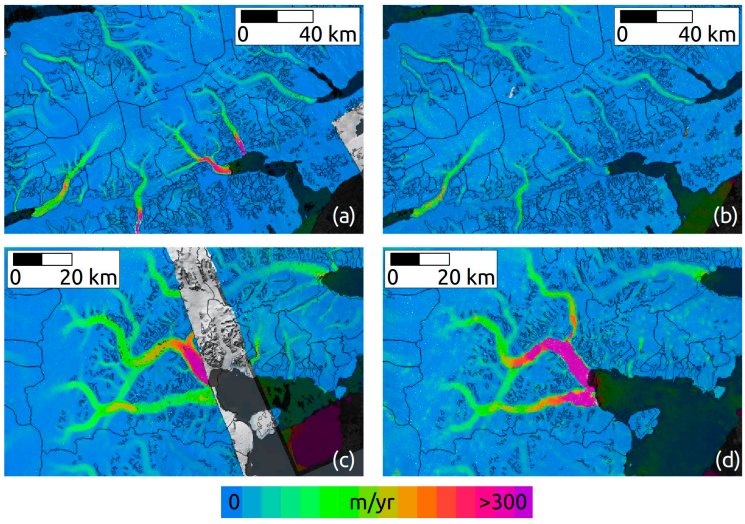

Figure 5. Close-up of the ice velocity maps for two areas on Ellesmere Island over the Canadian Arctic North from ALOS-1 PALSAR-1 winter data of 2007–2011 (**a**,**c**) and Sentinel-1 SAR winter data of 2015 (**b**,**d**).

Regular monitoring of the Svalbard archipelago with Sentinel-1 data is ongoing since mid August 2015, even if already during the ramp-up phase of the satellite in August 2014 and later on in January and February 2015 we were able to calculate first ice surface velocity maps. Time-series of ice surface velocities for the three active basins on the southeastern tip of Austfonna derived from Sentinel-1 data are shown on Figure 6d, highlighting the frequency of possible observations and processes to be studied. While for Basin-3 the surge was already active in the summer of 2014, for Basin-2 velocities were still lower at that time and increased significantly for the first time in the summer of 2015. The following winter velocities remained at a quite high level and a further increase in velocity was observed in the summer of 2016.

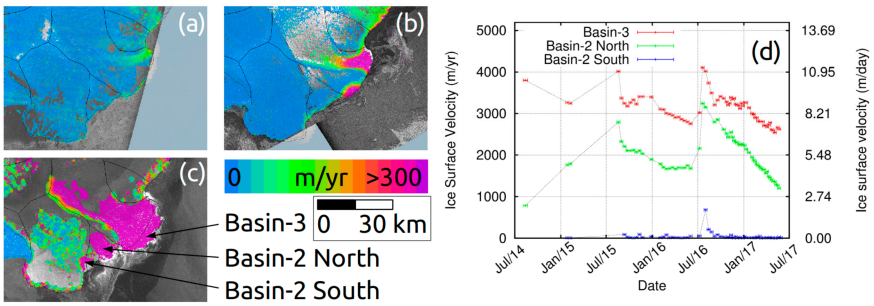

Figure 6. Ice surface velocity maps for the southeastern tip of Austfonna (Svalbard) from JERS-1 SAR data of 1998 (**a**), ALOS-1 PALSAR-1 data of 2010 (**b**) and Sentinel-1 from 26/07/2016 to 07/08/2016 (**c**) and time-series of Sentinel-1 velocity for Basin-3, Basin-2 North and Basin-2 South (**d**). The arrows point to the locations used for the time series.

Strozzi et al. [18] investigated the frontal destabilisation of Stonebreen over Edgeøya that started in 2011 in the detail. In Figure 7 we update the previously published data with latest results. As visible on two Sentinel-1 winter velocity maps of 2015 and 2017 (Figure 7a,b, respectively) there is in recent years a further surge expansion towards inland. In the time series of Figure 7c we observe that summer velocities close to the front were in 2016 decreasing in comparison to the maximum observed ones in 2015, but were still remaining at high levels.

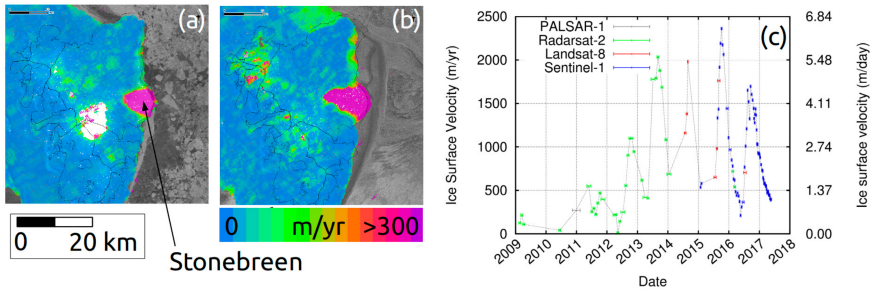

Figure 7. Ice surface velocity maps for Stonebreen on Edgeøya (Svalbard) from Sentinel-1 data of the time periods 21/01/2015 to 02/02/2015 (**a**) and 27/02/2017 to 11/03/2017 (**b**) and time-series of velocity close to the front from 2009 to 2017 (**c**).

The seasonally modulated time-series of ice surface velocity over Stonebreen with steadily increasing summer values over at least five years (Figure 7) is remarkably different from that measured over the same time period over Negribreen in the central-east of Spitsbergen (Figure 8). Negribreen was one of the largest surges in Svalbard that took place in 1935–1936 with an advance of almost 12 km into the fjord within one year along a 15 km wide section of the front [35]. For Negribreen we recognize in Figure 8c phase of a typical Svalbard glacier surge cycle [47], which starts with a years-long period of steady acceleration, followed by a months-long period of relatively rapid acceleration, a length of the active phase of typically 3–10 years, and a very gradual end of the fast flow phase with velocity

decreasing over a years-long period. The long active (~7–15 years) and quiescent (~50–100 years) phases, combined with surge termination that occurs over a multi-year period and velocity changes between the two phase of one or two orders of magnitude, suggest that the Svalbard-type surges are linked to changes in basal thermal conditions rather than subglacial water pressure [47]. Two Sentinel-1 velocity maps for October 2015 (Figure 8a) and October-November 2016 (Figure 8b) indicate that the surge front started in the lower part of the glacier and then migrated up-glacier.

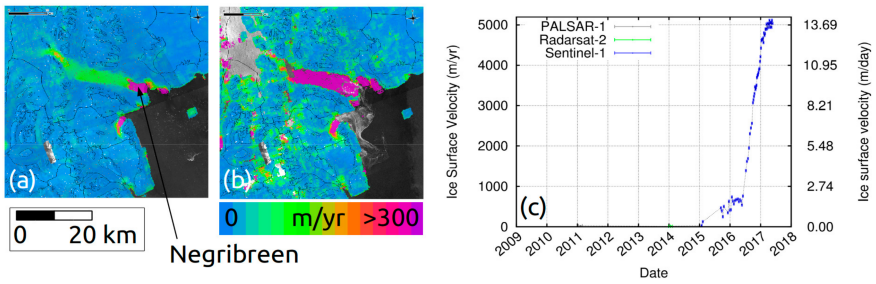

Figure 8. Ice surface velocity maps for Negribreen on Spitsbergen (Svalbard) from Sentinel-1 data of the time periods 01/10/2015 to 13/10/2015 (**a**) and 31/10/2016 to 12/11/2016 (**b**) and time-series of velocity close to the front from 2011 to 2017 (**c**). The arrow points to the location used for the time series.

Two other prominent recent surges on Spitsbergen are those of Penckbreen to the South of the island (Figure 9) and Strongbreen in the centre of the island (Figure 10). The comparison of two Sentinel-1 velocity maps for September–October 2015 (Figure 9a) and February 2017 (Figure 9b) for Penckbreen indicates that in this case the surge started in the centre of the glacier and then migrated up- and down-glacier. In the time-series of velocity from TerraSAR-X and Sentinel-1 data (Figure 9c) we recognize also for Penckbreen parts of the typical Svalbard glacier surge cycle [47], in particular the last part of a steady acceleration from 2012 to 2015, followed by a months-long period of relatively rapid acceleration at the end of 2015, and a gradual end of the fast flow phase afterwards. Also for Strongbreen the comparison of two Sentinel-1 velocity maps for September 2015 (Figure 10a) and February 2017 (Figure 10b), even if quite noisy because of the relatively small size of the glacier, indicates that the surge started in the central-upper part of the glacier and then migrated down-glacier. In the time-series of velocity from Sentinel-1 data (Figure 10c) the very rapid acceleration at the end of 2015 has strong similarities with that observed for Negribreen (Figure 8c) with highest velocities peaking at about 5000 m/year (or 14 m/day). Animations of the Sentinel-1 backscattering intensity images, available as Supplementary Material, can be employed to visually follow the evolution of a surge. In the case of Strongbreen (Video S4) we observe the start of the surge in the central part of the glacier around September 2016, followed after November 2016 and until present by a prominent advance of the front of the glacier into the fjord. Also for Negribreen (Video S2) the start of the surge and the advance of the front into the fjord can be very well followed in the animation of the Sentinel-1 backscattering intensity images from January 2015 to May 2017. In this case, the surge started at the front. For Penckbreen (Video S3) the surge started in the centre of the glacier and the glacier front did not reach the fjord during its advancing phase until May 2017.

The comparison of Figure 9a,b also nicely shows the end of the surge of the Nathorstbreen glacier system, which started in 2009 with a frontal advance of about 15 km [17]. In order to further characterize the spatio-temporal dynamic pattern of this glacier system we compare in Figure 11a,b and c the ice surface displacement maps derived in 1994 from JERS-1 SAR, in 2012 from TerraSAR-X and in 2015/2016 from Sentinel-1, respectively. The gradual end of the fast flow phase is well picked-up by the time-series of Sentinel-1 velocities from 2015 to 2017, where superimposed to the deceleration trend we also observe prominent summer speed-ups in 2015 and 2016.

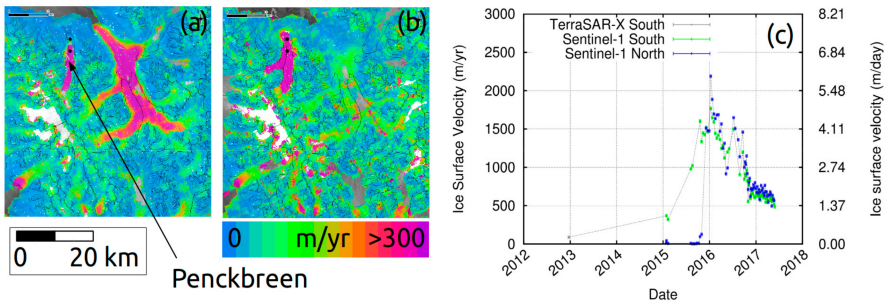

Figure 9. Ice surface velocity maps for Penckbreen on South Spitsbergen (Svalbard) from Sentinel-1 data of the time periods 19/09/2015 to 01/10/2015 (**a**) and 16/02/2017 to 28/02/2017 (**b**) and time-series of velocity for two points (labelled as South and North with respect to their latitude) from 2012 to 2017 (**c**). The two dots indicate the locations used for the time series.

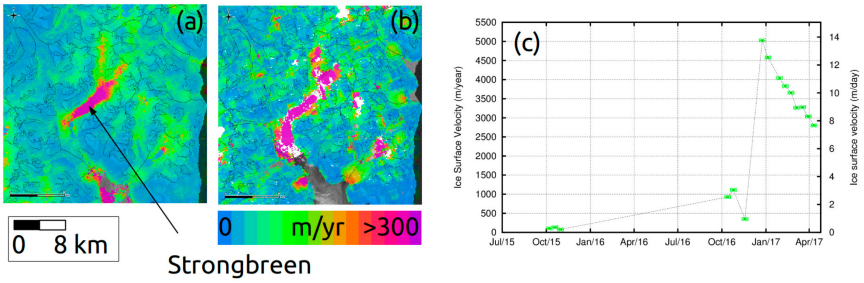

Figure 10. Ice surface velocity maps for Strongbreen on Spitsbergen (Svalbard) from Sentinel-1 data of the time periods 19/09/2015 to 01/10/2015 (**a**) and 16/02/2017 to 28/02/2017 (**b**) and time-series of Sentinel-1 velocity (**c**). The arrow points to the location used for the time series.

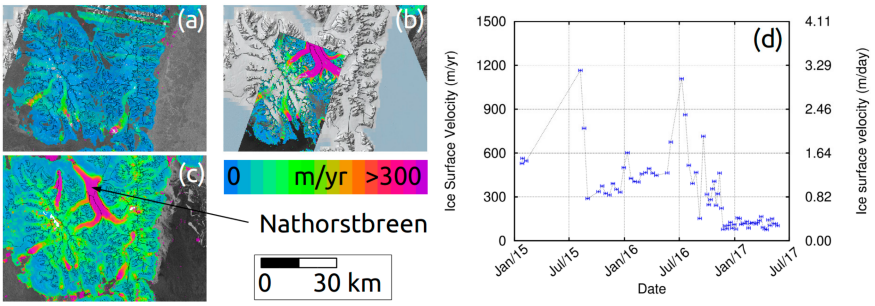

Figure 11. Ice surface velocity maps for Nathorstbreen on South Spitsbergen (Svalbard) from JERS-1 SAR in 1994 (**a**), TerraSAR-X in 2012 (**b**) and Sentinel-1 in 2015/2016 (average of winter data, (**c**)) and Sentinel-1 time-series of velocity from 2015 to 2017 (**d**). The arrow points to the location used for the time series.

For many other glaciers over the Svalbard Archipelgo a steady increase of frontal velocities along with a retreat of frontal positions is observed. Figure 12 shows for instance velocity maps for the northeastern tip of Austfonna (Svalbard) from the winter of 2008, 2015 and 2017. An increase in ice velocity is evident in recent years at the glacier's fronts, even if there is so far no advance of the calving front. A distinct acceleration can be observed in July 2016, and velocities were increasing again until the beginning of the 2017 winter.

3.4. Variability of Glacier Dynamics in the Russian Arctic

Frontal velocities over Novaya Zemlya glaciers were generally higher in 2016 compared to 2008–2010, in particular along the Barents Sea coast (Figure 4d). As previously observed by [14,22], marine-terminating

glaciers along the Barents Sea coast have the highest frontal velocities on Novaya Zemlya (Figures 2d and 3d). As shown in the close-up of Figure 13, results from JERS-1 SAR of 1998, ALOS-1 PALSAR-1 of 2008–2009 and Sentinel-1 of 2016 indicate a general steady increase of frontal velocities along with a retreat of frontal positions. This is in agreement with the conclusions of [14] regarding summer terminus speeds and frontal positions determined from 2006 to 2012 with tracking of satellite optical and SAR data. Over the interior of the ice cap we observe low quality Sentinel-1 results (Figure 13f), while the JERS-1 SAR (Figure 13d) and ALOS-1 PALSAR-1 map (Figure 13e) have a better spatial coverage. The greater penetration of the radar signals into the snow and firn at L-band compared to C-band [48] results in a reduced decorrelation. A dedicated ALOS-2 PALSAR-2 acquisition campaign with winter stripmap data would allow to derive a more complete coverage in the interior of the ice cap also for recent years. As an alternative, increasing the temporal sampling of Sentinel-1 acquisitions to 6 days would possibly also improve the spatial coverage.

Frontal velocities over glaciers on Franz-Josef Land were generally higher in 2016 compared to 1998–2011, in particular to the south-east of the Archipelago (Figure 4e). Analysis of the SAR backscattering intensity images also indicates a general retreat of frontal positions in recent years, as previously described for Novaya Zemlya. Simony Glacier on McClintock Island is an exception to this trend. As indicated in Figure 14, over this glacier we observe from 1998 to 2015 an advance of the glacier along with an increase in frontal velocities. Satellite optical images were considered to further analyse this area. The crevassed area of the glacier was larger in 2014 (Figure 14d) than in 2006 (Figure 14c). We hypothesize that this glacier might have undergone a frontal destabilisation similar to what was previously described for Stonebreen on Edgeøya (Figure 7). Unfortunately, over Franz-Josef Land, there were until recent no regular acquisitions of satellite SAR images available to compute a long time-series of ice surface velocity.

The comparison of ice surface velocities over Severnaya Zemlya between 2010 and 2016 (Figure 4f) is difficult, because the results from summer ALOS-1 PALSAR-1 data have limited spatial coverage. However, we recognize also over this region a general steady increase of frontal velocities along with a retreat of frontal positions. The western margin of the Vavilov Ice Cap on October Revolution Island is a very prominent exception to this trend. Over the Vavilov Ice Cap we observe since 2015 a strong increase in ice surface velocity along with a very strong advance in frontal extension, as previously reported by [23]. We captured the changes in velocities over the Vavilov Ice Cap from ALOS-1 PALSAR-1, ALOS-2 PALSAR-2 ScanSAR, Sentinel-1 and Radarsat-2 Wide Ultra Fine (WUF) data (Figure 15). As observed over Basin-3 [5,15] or Stonebreen [18] also over the Vavilov Ice Cap the surge started at the glacier front and migrated up-glacier afterwards. The increase in velocity is very strong, up to the summer of 2016 values of almost 7000 m/year (i.e., almost 20 m/day) were observed. During autumn and winter 2016/2017 there is a decrease of velocities, as previously observed over Basin-3 [5], Basin-2 (Figure 6d) or Stonebreen (Figure 7c). The satellite optical images of summer of 2010 (Figure 15a) and 2016 (Figure 15b) nicely show the advance of the glacier into the sea in recent years.

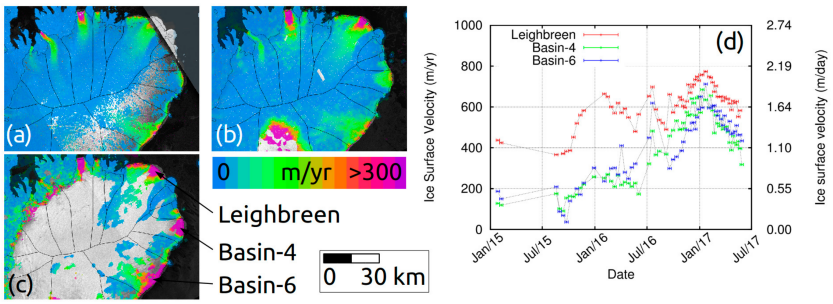

Figure 12. Ice surface velocity maps for the north-eastern tip of Austfonna (Svalbard) from ALOS-1 PALSAR-1 in 2008 (**a**), Sentinel-1 from 21/01/2015 to 02/02/2015 (**b**) and Sentinel-1 from 17/03/2017 to 29/03/2017 (**c**) and Sentinel-1 time-series of velocity for three glacier fronts from 2015 to 2017 (**d**). The arrows point to the locations used for the time series.

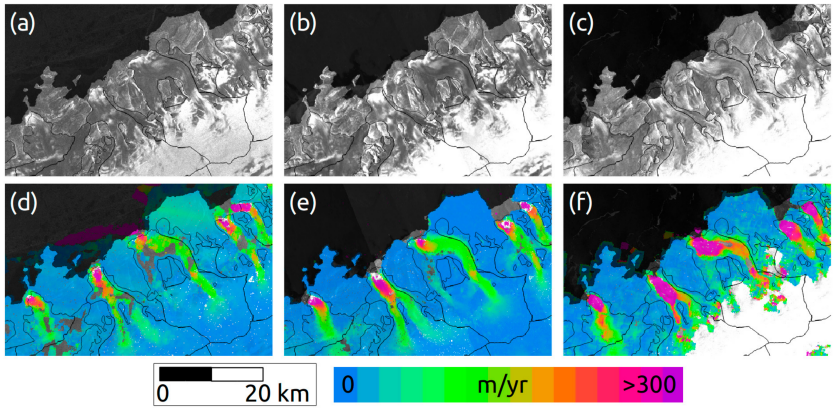

Figure 13. JERS-1 SAR 1998 backscattering intensity image and velocity map (**a**,**d**) ALOS-1 PALSAR-1 2009/2010 backscattering intensity image and velocity map (**b**,**e**) and Sentinel-1 2016 backscattering intensity image and velocity map (**c**,**f**) over marine-terminating glaciers along the Barents Sea coast of Novaya Zemlya.

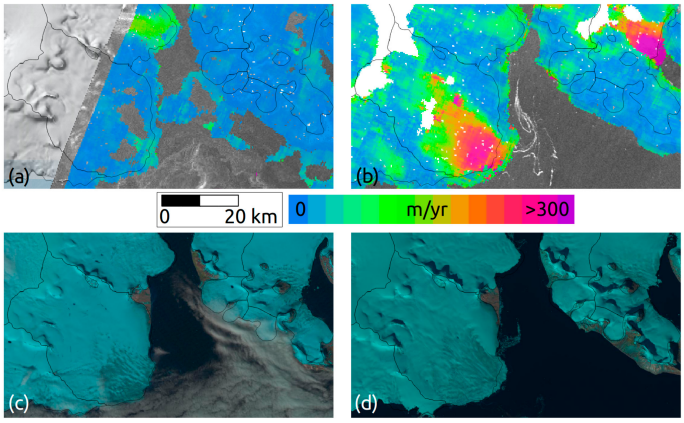

Figure 14. Ice surface velocity maps for Simony Glacier on McClintock Island (Franz Josef Land) from JERS-1 SAR data in 1998 (**a**) and Sentinel-1 in October 2015 (**b**) and satellite optical images from Landsat-4 on 22/07/2006 (**c**) and Landsat-8 on 27/08/2014 (**d**).

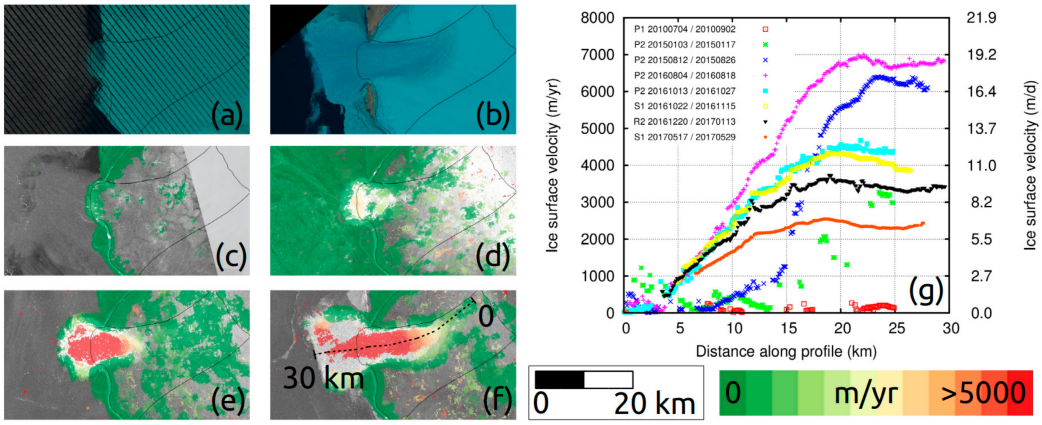

Figure 15. Vavilov Ice Cap (Severnaya Zemlya): satellite optical images from Landsat-7 on 07-09-2010 (**a**) and Landsat-8 on 15-07-2016 (**b**), ice surface velocity maps from ALOS-1 PALSAR-1 in 2010 (**c**), ALOS-2 PALSAR-2 in January 2015 (**d**), ALOS-2 PALSAR-2 in August 2015 (**e**) and ALOS-2 PALSAR-2 in August 2016 (**f**), and time-series of surface displacements on a profile along the centre flow-line of the glacier from ALOS-1 PALSAR-1 (P1), ALOS-2 PALSAR-2 (P2), Sentinel-1 (S1) and Radarsat-2 (R2) data (**g**).

4. Discussion

4.1. Error Assessment

An assessment of the uncertainties in the ice displacement maps is essential for the interpretation of changes in glacier dynamics, but is inherently difficult because glacier surface velocities are variable temporally and spatially [49]. For an estimation of the error we compare our satellite-derived displacement maps with products derived from independent image data of better resolution and precision. Studies performed along these lines in the past with JERS-1 SAR data separated by a repeat-cycle of 44 days [22] and ALOS-1 PALSAR-1 data separated by a repeat-cycle of 46 days [25] indicated expected errors of about $\pm$20 and $\pm$10 m/year, respectively. Here we specifically evaluate the performance of Sentinel-1 over Svalbard and Severnaya Zemlya glaciers using Radarsat-2 WUF data characterised by a spatial resolution of about 3 m, a time interval of 24 days, and a coverage of approximately 50 km $\times$ 50 km. In addition, Sentinel-1 data are compared to ground-based radar measurements with a spatial resolution of about 2 m $\times$ 16 m over Kronebreen (Svalbard).

The uncertainty of the ice surface velocity product is estimated as the mean and standard deviation between the differences from the "true" velocity (Radarsat-2 or ground-based radar) to the velocity measured with Sentinel-1. The discrepancy between the products is thus a function of the accuracy of both matches, the spatial representativeness of the displacement compared to the "real" displacement, and the temporal variations between the acquisition dates of the two sets of images. For Radarsat-2 WUF data the estimated displacement error is ~$\pm$5 m/year by assuming a precision of 1/20th of a pixel in the offset estimation. For the ground-based radar interferometer, with images acquired every 2 min over 3 h, the velocity uncertainty is 0.05 m/day (18 m/year) or less [50].

Ice surface velocity maps computed from Radarsat-2 WUF mode over Basin-2 and Basin-3, Stonebreen (all on Svalbard) and the Vavilov Ice Cap (Severnaya Zemlya) were inter-compared with ice surface velocity maps computed from Sentinel-1 of very similar but not exactly coincident time intervals (see Supplementary Table S1 for information about the image dates). The results of the inter-comparison exercise are listed in Table 2, where a separation between regions close to glacier's calving fronts and shear zones, where spatial and temporal variability of ice surface velocity is large, and regions far from glacier calving fronts and shear zones is introduced.

On average, the mean difference and standard deviation between the Radarsat-2 and Sentinel-1 ice velocity records for areas far from the glacier calving fronts and shear zones were 17 m/year and 26 m/year, respectively. For areas close to Basin-2, Basin-3 and Stonebreen calving fronts and shear zones the mean difference and standard deviation between the Radarsat-2 and Sentinel-1 ice velocity records were on average 38 m/year and 64 m/year, respectively. Ice surface velocities during winter 2016 over Basin-2 and Basin-3 were over 2000 m/year, over Stonebreen up to 1000 m/year. The maps and profiles of Figure 16 over Stonebreen illustrate the good match between the Sentinel-1 and Radarsat-2 image pairs. In general the flow structures over the highly crevassed surging glacier are better captured by the higher resolution Radarsat-2 data. For the surging Vavilov Ice Cap glacier, the mean difference and standard deviation between the Radarsat-2 and Sentinel-1 ice velocity records were $-$2 m/year and 63 m/year, respectively. Again, the maps and profiles of Figure 17 indicate how Radarsat-2 data better captures the fine flow structures over the highly crevassed surging glacier, whereas the Sentinel-1 velocity map is smoother.

Table 2. Results of the validation of ice surface velocity products.

Inter-Comparison Experiment	Mean Difference	Standard Deviation
Regions far from glacier calving fronts and shear zones		
Radarsat-2 WUF Mode Basin-2, Basin-3 and Stonebreen	17 m/year	26 m/year
GPRI-2 Kronebreen (3 h)	8 m/year	22 m/year
Regions close to glacier calving fronts and shear zones		
Radarsat-2 WUF Mode Basin-2, Basin-3 and Stonebreen	38 m/year	64 m/year
Radarsat-2 WUF Mode Vavilov Ice Cap	$-$2 m/year	63 m/year
GPRI-2 Kronebreen (3 h)	67 m/year	268 m/year

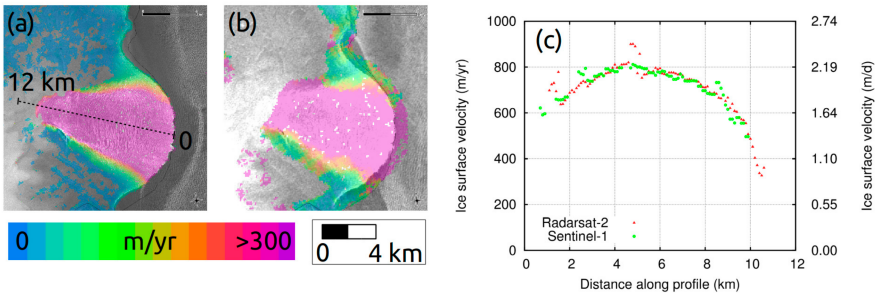

Figure 16. Ice velocity maps on Stonebreen (Svalbard) from (**a**) Radarsat-2 WUF data of 04/28-02-2016 and (**b**) Sentinel-1 data of 09/21-02-1016 and (**c**) inter-comparison along the centre flow line plotted in (**a**).

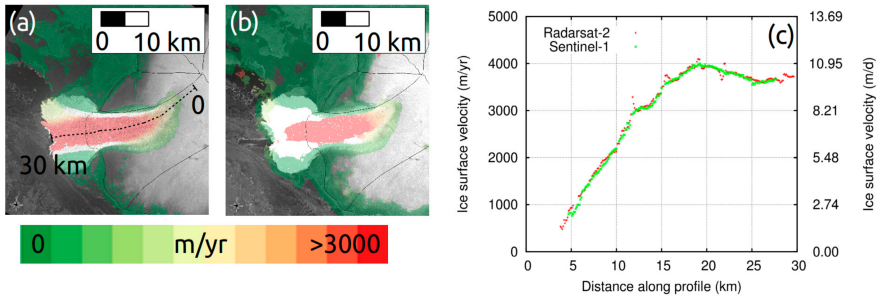

Figure 17. Ice velocity maps on Vavilov Ice Cap (Severnaya Zemlya) from (**a**) Radarsat-2 WUF data of 26-11/20-12-2016 and (**b**) Sentinel-1 data of 30-11/12-12-1016 (**c**) and inter-comparison alongthe centre flow line plotted in (**a**).

Ground-based radar measurements of ice surface velocity around the front of Kronebreen (Svalbard) were performed with Gamma Portable Radar Interferometers (GPRI, [50]) during 3 h on 27 August 2016 simultaneously from two locations on both sides of the fjord. The two line-of-sight measurements were combined to derive horizontal ice surface velocity (Figure 18). Information from the ground-based systems is limited by extensive shadow and restricted to the front of the glacier and a few other smaller areas further upwards. Inter-comparison with the Sentinel-1 ice surface velocity map computed with acquisitions of 20 August and 1 September 2016 for a region away from the calving front and shear zones (region 1 in Figure 18) indicated a mean difference and standard deviation between the two records of 8 m/year and 22 m/year, respectively. Mean velocities over this homogeneously moving area were 417 m/year from the GPRI-2 records and 405 m/year for the Sentinel-1 records, respectively. Close to the calving front (region 2 in Figure 18) mean difference and standard deviation between the two records were 67 m/year and 268 m/year, respectively, and mean velocities were 581 m/year from the GPRI-2 records and 552 m/year for the Sentinel-1 records, respectively. At the calving front Sentinel-1 ice surface velocities are underestimated and the uncertainty gets larger, because fast-moving spots at the glacier's front, well visible from the in situ records (Figure 18a), are mixed with areas of much lower velocity in the large windows used for the satellite image correlation (Figure 18b).

The overall uncertainty of the ice surface velocity products derived from Sentinel-1 data with a time interval of 12 days estimated from our inter-comparison exercises in areas far from relatively small glacier's calving fronts and shear zones is between ±20 and ±30 m/year (±0.05 to ±0.08 m/day). These numbers correspond well to the statistical measures of ice surface velocity that are computed for every individual Sentinel-1 frame over ice-free regions. In addition, by assuming a precision of 1/20th of a pixel in the offset estimation, the displacement error of Sentinel-1 IWS data with pixel sizes in ground-range and azimuth direction of 8 m × 20 m, respectively, and a time interval of 12 days is also on the order of 30 m/year. Similar ice surface velocity products derived from Sentinel-1 image pairs were compared by [29] to ice velocity maps retrieved from TerraSAR-X data on the Greenland

west coast. The uncertainty for slow moving areas between 0.1 and 0.5 m/day (35 to 180 m/year) of Sentinel-1 velocities retrieved from single image pairs was estimated to ±0.068 m/day (±25 m/year).

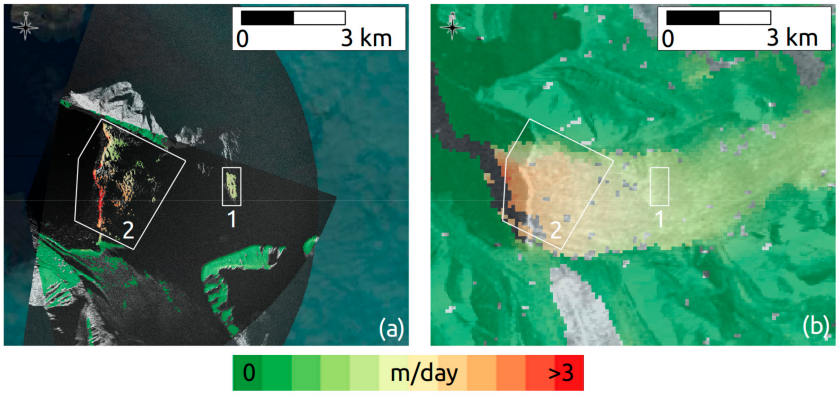

Figure 18. Ice velocity maps over Kronebreen (Svalbard) from GPRI data of 27-08-2016 (**a**) and Sentinel-1 data of 20-08/01-09-2016 (**b**). The two boxes indicate the regions where the inter-comparison in performed.

Finally, for an assessment of the error of the velocity maps derived from ALOS-2 PALSAR-2 ScanSAR data over Severnaya Zemlya we consider statistical measures over ice-free regions. The performance of this image data set is poor, the standard deviation of the estimates over ice-free regions is often larger than 200 m/year, but because the ice surface velocities over the Vavilov Ice Cap in 2016 were extremely large (>5000 m/year) these products could also be considered in our analysis.

4.2. Interpretation of Results

Ice velocity maps computed with satellite SAR data for large islands over the Canadian Arctic, Svalbard and the Russian Arctic for at least two points in time during the last 20 years highlighted regional-scale trends, interrupted by a number of glaciers where dramatic changes are ongoing. Gradual slow-down dominates over many glaciers in the Canadian High Arctic, while steady increase of frontal velocities along with a retreat of frontal positions is common for many glaciers over the Svalbard archipelago and the Russian Arctic. From our velocity measurements alone we cannot conclude about the causes of this regionally contrasted behaviour (mass balance, ocean influences or other). However, our results underline that instabilities or flow variations of a few large glaciers, interrupting the above general regional pattern, dominate the total calving flux from Arctic ice caps and glaciers. Estimation of climate change impacts through large Arctic glaciers is thus complicated. Many glaciers in the Arctic might respond more or less directly to climatic forcing and thus exhibit general region-specific trends. However, the destabilisation of large glaciers or considerable velocity variation of fast-flowing basins involves complex and typically sub-glacial mechanisms and feedbacks that are so far only partially understood.

We followed these changes practically in real time with Sentinel-1, which now enables very high temporal resolution observations from 6 to 12 days even if at coarse spatial resolution. We notice that, in recent years, over Eastern Svalbard and the Russian Arctic there seems to be a trend of an increasing number of glaciers with frontal destabilization compared to the 1990s, while over the Canadian Arctic changes are minor. Such suggestion is based on only a few velocity snapshots, and more observations and calculations would be necessary to reliably conclude about an increase in Arctic glacier destabilizations. Though, environmental changes in the Arctic are pronounced, not least through the reduction of sea ice cover and its consequences, and it is well expected that Arctic glaciers adjust to these changes. One mechanism how climatic changes may affect glacier dynamics relatively fast was proposed by [5], who suggested a hydro-thermodynamic feedback where increased melt-water production and input to the glacier bed is able to stepwise trigger a surge-type instability.

5. Conclusions and Perspectives

We demonstrated how recent SAR satellites, in particular the Sentinel-1 constellation, enable year-round and operational ice surface velocity estimation for Arctic glaciers and ice caps. In general, we observed that changes in the flow of glaciers and ice caps observed between the 1990s and 2017 over the Canadian Arctic are minor compared to those observed over Svalbard and the Russian Arctic. While a gradual slow-down dominates over many glaciers in the Canadian High Arctic, a steady increase of frontal velocities along with a retreat of frontal positions is common for many glaciers over the Svalbard archipelago and the Russian Arctic. However, in all regions this general pattern is interrupted by a number of glaciers where strong accelerations are ongoing. The fact that, largely unexpected, destabilizations of a few glaciers are able to dominate the total calving flux and thus sea-level impact from Arctic glaciers and ice caps, at least over time-scales of years to decades, underlines how important it is to have a reliable, accurate and automatic, all-weather and year-round satellite-based glacier velocity monitoring system available.

At present, regular acquisitions at high temporal sampling from the two Sentinel-1 satellites combined with the availability of high-resolution DEM's and processing tools and resources enable us to automatically produce mosaics and time-series of ice surface velocity with accuracies of 20 to 30 m/year. Similar work based on optical satellite sensors (e.g., [27,31]) perfectly complements the regular SAR-derived velocity maps by providing higher spatial resolution of results in cloud-free conditions during the Arctic summer. We plan to continue near-real time processing with Sentinel-1 over the Arctic and to complement, where feasible, ice surface velocity information with glaciers' frontal positions, elevation changes and bathymetry at the calving fronts. Sentinel-1 is remarkably augmenting our capacity to capture the spatial and temporal evolution of glacier surges. This significant information can be further used to constrain numerical models of glacier flow to better understand reasons and mechanisms of surges or frontal destabilisation processes and possibly predict the temporal evolution of the contribution of Arctic glaciers to sea level rise.

Supplementary Materials: The following are available online at www.mdpi.com/2072-4292/9/9/947/s1, Table S1: Sensors, acquisition dates and time intervals of the satellite SAR image pairs considered for ice surface velocity estimation over the different study regions, Video S2: Animation of the Sentinel-1 backscattering intensity images for Negribreen (Svalbard), Video S3: Animation of the Sentinel-1 backscattering intensity images for Penckbreen (Svalbard), Video S4: Animation of the Sentinel-1 backscattering intensity images for Strongbreen (Svalbard).

Acknowledgments: The research leading to these results received funding from the European Space Agency (ESA) within the Glaciers_cci project (code 4000109873/14/I-NB), the European Union Seventh Framework Program (FP7) under grant agreements No. 607052 (SEN3APP project), the European Research Council (ERC) under contract ID 320816 (ICEMASS project), the Norwegian Space Centre under contract NIT.06.15.5, and the Research Council of Norway under contract 244196/E10 (CalvingSEIS project). ALOS-1 PALSAR-1 images provided by ESA (courtesy of AOPOL.4086), the Japan Aerospace Exploration Agency (JAXA, courtesy of RA6-3016) and the Alaska Satellite Facility (ASF). Sentinel-1 and Radarsat-2 Wide Ultra Fine images available from Copernicus. JERS-1 SAR data provided by ESA, courtesy of C1P.2611. Radarsat-2 Wide Mode data provided by NSC/KSAT under the Norwegian-Canadian Radarsat agreement. ALOS-2 PALSAR-2 provided by JAXA, courtesy of RA6-3016. Landsat data available from the U.S. Geological Survey. TanDEM-X data provided by the German Aerospace Center (DLR), courtesy of Wegmulle_NTI_INSA3397.

Author Contributions: T.S., F.P. and A.K. designed the experiments; T.S. and A.W. processed most of the satellite SAR images, T.S. contributed with the analysis of Radarsat-2 images over Svalbard; T.S. led the writing of the paper; all authors analysed the results and contributed to the redaction of the paper.

Conflicts of Interest: The authors declare no conflict of interest.

References

1. Pfeffer, W.T.; Arendt, A.A.; Bliss, A.; Bolch, T.; Cogley, J.G.; Gardner, A.S.; Hagen, J.O.; Hock, R.; Kaser, G.; Kienholz, C.; et al. The Randolph Glacier Inventory: A globally complete inventory of glaciers. *J. Glaciol.* **2014**, *60*, 537–552. [CrossRef]
2. Vaughan, D.G.; Comiso, J.C.; Allison, I.; Carrasco, J.; Kaser, G.; Kwok, R.; Mote, P.; Murray, T.; Paul, P.; Ren, J. Observations: Cryosphere. In *Climate Change 2013: The Physical Science Basis. Contribution of Working*

Group I to the Fifth Assessment Report of the Intergovernmental Panel on Climate Change; Stocker, T.F., Qin, D., Plattner, G.-K., Tignor, M.M.B., Allen, S.K., Boschung, J., Nauels, A., Xia, Y., Bex, V., Midgley, P.M., Eds.; Cambridge University Press: Cambridge, UK; New York, NY, USA, 2013.

3. Church, J.; Clark, P.; Cazenave, A.; Gregory, J.; KhanJevrejeva, S.A.; Levermann, A.; Merrifield, M.; Milne, G.; Nerem, R.; Nunn, P.; et al. Sea Level Change. In *Climate Change 2013: The Physical Science Basis. Contribution of Working Group I to the Fifth Assessment Report of the Intergovernmental Panel on Climate Change*; Stocker, T.F., Qin, D., Plattner, G.-K., Tignor, M.M.B., Allen, S.K., Boschung, J., Nauels, A., Xia, Y., Bex, V., Midgley, P.M., Eds.; Cambridge University Press: Cambridge, UK; New York, NY, USA, 2013.
4. Zekollari, H.; Huybrechts, P.; Noël, B.; van de Berg, W.J.; van den Broeke, M. Sensitivity, stability and future evolution of the world's northernmost ice cap, Hans Tausen Iskappe (Greenland). *Cryosphere* **2017**, *11*, 805–825. [CrossRef]
5. Dunse, T.; Schellenberger, T.; Hagen, J.-O.; Kääb, A.; Schuler, T.; Reijmer, C. Glacier-surge mechanisms promoted by a hydro-thermodynamic feedback to summer melt. *Cryosphere* **2015**, *9*, 197–215. [CrossRef]
6. Paterson, W.S.B. *The Physics of Glaciers*, 3rd ed.; Pergamon: New York, NY, USA, 1994; p. 480.
7. Huss, M.; Farinotti, D. A high-resolution bedrock map for the Antarctic Peninsula. *Cryosphere* **2014**, *8*, 1261–1273. [CrossRef]
8. Millan, R.; Mouginot, J.; Rignot, E. Mass budget of the glaciers and ice caps of the Queen Elizabeth Islands, Canada, from 1991 to 2015. *Environ. Res. Lett.* **2017**, *12*, 2. [CrossRef]
9. Gardner, A.; Moholdt, G.; Wouters, B.; Wolken, G.; Burgess, D.; Sharp, M.; Cogley, J.; Braun, C.; Labine, C. Sharply increased mass loss from glaciers and ice caps in the Canadian Arctic Archipelago. *Nature* **2011**, *473*, 357–360. [CrossRef] [PubMed]
10. Gardner, A.; Moholdt, G.; Arendt, A.; Wouters, B. Accelerated contributions of Canada's Baffin and Bylot Island glaciers to sea level rise over the past half century. *Cryosphere* **2012**, *6*, 1103–1125. [CrossRef]
11. Van Wychen, W.; Copland, L.; Gray, L.; Burgess, D.; Danielson, B.; Sharp, M. Spatial and temporal variation of ice motion and ice flux from Devon Ice Cap, Nunavut, Canada. *J. Glaciol.* **2012**, *580*, 657–664. [CrossRef]
12. Van Wychen, W.; Copland, L.; Burgess, D.; Gray, L.; Schaffer, N. Glacier velocities and dynamic discharge from the ice masses of Baffin Island and Bylot Island, Nunavut, Canada. *Can. J. Earth Sci.* **2015**, *52*, 980–989. [CrossRef]
13. Van Wychen, W.; Davis, J.; Burgess, D.; Copland, L.; Gray, L.; Sharp, M.; Mortimer, C. Characterizing interannual variability of glacier dynamics and dynamic discharge (1999–2015) for the ice masses of Ellesmere and Axel Heiberg Islands, Nunavut, Canada. *J. Geophys. Res. Earth Surf.* **2016**, *121*, 39–63. [CrossRef]
14. Melkonian, A.; Willis, M.; Pritchard, M.; Stewart, A. Recent changes in glacier velocities and thinning at Novaya Zemlya. *Remote Sens. Environ.* **2016**, *174*, 244–257. [CrossRef]
15. McMillan, M.; Shepherd, A.; Gourmelen, N.; Dehecq, A.; Leeson, A.; Ridout, A.; Flament, T.; Hogg, A.; Gilbert, L.; Benham, T.; et al. Rapid dynamic activation of a marine-based Arctic ice cap. *Geophys. Res. Lett.* **2014**, *41*, 8902–8909. [CrossRef]
16. Schellenberger, T.; Van Wychen, W.; Copland, L.; Kääb, A.; Gray, L. An Inter-Comparison of Techniques for Determining Velocities of Maritime Arctic Glaciers, Svalbard, Using Radarsat-2 Wide Fine Mode Data. *Remote Sens.* **2016**, *8*, 785. [CrossRef]
17. Sund, M.; Lauknes, T.R.; Eiken, T. Surge dynamics in the Nathorstbreen glacier system, Svalbard. *Cryosphere* **2014**, *8*, 623–638. [CrossRef]
18. Strozzi, T.; Kääb, A.; Schellenberger, T. Frontal destabilisation of Stonebreen, Edgeøya, Svalbard. *Cryosphere* **2017**, *11*, 553–566. [CrossRef]
19. Schellenberger, T.; Dunse, T.; Kääb, A.; Schuler, T.; Hagen, J.-O.; Reijmer, C. Multi-year surface velocities and sea-level rise contribution of the Basin-3 and Basin-2 surges, Austfonna, Svalbard. *Cryosphere Discuss.* **2017**. [CrossRef]
20. Luckman, A.; Benn, D.; Cottier, F.; Bevan, S.; Nilsen, F.; Inall, M. Calving rates at tidewater glaciers vary strongly with ocean temperature. *Nat. Commun.* **2015**, *6*, 8566. [CrossRef] [PubMed]
21. Dowdeswell, J.; Bassford, R.; Gorman, M.; Williams, M.; Glazovsky, A.; Macheret, Y.; Shepherd, A.; Vasilenko, Y.; Savatyuguin, L.; Hubberten, H.-W.; et al. Form and flow of the Academy of Sciences Ice Cap, Severnaya Zemlya, Russian High Arctic. *J. Geophys. Res.* **2002**, *107*, 2076. [CrossRef]
22. Strozzi, T.; Kouraev, A.; Wiesmann, A.; Wegmüller, U.; Sharov, A.; Werner, C. Estimation of Arctic glacier motion with satellite L-band SAR data. *Remote Sens. Environ.* **2008**, *112*, 636–645. [CrossRef]

23. Glazovsky, A.; Bushueva, I.; Nosenko, G. "Slow" surge of the Vavilov Ice Cap, Severnaya Zemlya. In Proceedings of the IASC Workshop on the Dynamics and Mass Balance of Arctic Glaciers, Obergurgl, Austria, 23–25 March 2015.
24. Strozzi, T.; Luckman, A.; Murray, T.; Wegmüller, U.; Werner, C. Glacier motion estimation using SAR offset-tracking procedures. *IEEE Trans. Geosci. Remote Sens.* **2002**, *40*, 2384–2391. [CrossRef]
25. Paul, P.; Bolch, T.; Kääb, A.; Nagler, T.; Nuth, C.; Scharrer, K.; Shepherd, A.; Strozzi, T.; Ticconi, F.; Bhambri, R.; et al. The glaciers climate change initiative: Methods for creating glacier area; elevation change and velocity products. *Remote Sens. Environ.* **2015**, *162*, 408–426. [CrossRef]
26. Dehecq, A.; Gourmelen, N.; Trouve, E. Deriving large-scale glacier velocities from a complete satellite archive: Application to the Pamir-Karakoram-Himalaya. *Remote Sens. Environ.* **2015**, *162*, 55–66. [CrossRef]
27. Fahnestock, M.; Scambos, T.; Moon, T.; Gardner, A.; Haran, T.; Klinger, M. Rapid large-area mapping of ice flow using Landsat 8. *Remote Sens. Environ.* **2016**, *185*, 84–94. [CrossRef]
28. Burgess, E.; Forster, R.; Larsen, C. Flow velocities of Alaskan glaciers. *Nat. Commun.* **2013**, *4*, 2146. [CrossRef] [PubMed]
29. Nagler, T.; Rott, H.; Hetzenecker, M.; Wuite, J.; Potin, P. The Sentinel-1 Mission: New Opportunities for Ice Sheet Observations. *Remote Sens.* **2015**, *7*, 9371–9389. [CrossRef]
30. Heid, T.; Kääb, A. Repeat optical satellite images reveal widespread and long term decrease in land-terminating glacier speeds. *Cryosphere* **2012**, *6*, 467–478. [CrossRef]
31. Kääb, A.; Winsvold, S.H.; Altena, B.; Nuth, C.; Nagler, T.; Wuite, J. Glacier remote sensing using Sentinel-2. Part I: Radiometric and geometric performance, and application to ice velocity. *Remote Sens.* **2016**, *8*, 598. [CrossRef]
32. Altena, B.; Kääb, A. Elevation change and improved velocity retrieval using orthorectified optical satellite data from different orbits. *Remote Sens.* **2017**, *9*, 300. [CrossRef]
33. Arendt, A.; Bliss, A.; Bolch, T.; Cogley, J.G.; Gardner, A.S.; Hagen, J.-O.; Hock, R.; Huss, M.; Kaser, G.; Kienholz, C. *Randolph Glacier Inventory—A Dataset of Global Glacier Outlines: Version 5.0. Global Land Ice Measurements from Space*; Digital Media: Boulder Colorado, CO, USA, 2015.
34. Dunbar, M.J.; Adams, P.R. The Canadian Encyclopedia. Arctic Archipelago. 2006. Available online: http://www.thecanadianencyclopedia.ca/en/article/arctic-archipelago (accessed on 31 May 2017).
35. Lefauconnier, B.; Hagen, J.-O. *Surging and Calving Glaciers in Eastern Svalbard*; Meddelelser Nr. 116; Norsk Polarinstitutt: Oslo, Norway, 1991.
36. Martín-Moreno, R.; Allende Álvarez, F.; Hagen, J.-O. 'Little Ice Age' glacier extent and subsequent retreat in Svalbard archipelago. *Holocene* **2017**, 1–12. [CrossRef]
37. Hagen, J.-O.; Liestøl, O.; Roland, E.; Jørgensen, T. *Glacier Atlas of Svalbard and Jan Mayen (Meddelelser 129)*; Norsk Polarinstitutt: Oslo, Norway, 1993.
38. Nordli, Ø.; Przybylak, R.; Ogilvie, A.; Isaksen, K. Long-term temperature trends and variability on Spitsbergen: The extended Svalbard Airport temperatures series, 1898–2012. *Polar Res.* **2014**, *33*, 21349. [CrossRef]
39. Rastner, P.; Strozzi, T.; Paul, F. Fusion of multi-source satellite data and DEMs to create a new glacier inventory for Novaya Zemlya. *Remote Sens.* **2017**, in review.
40. Moholdt, G.; Wouters, B.; Gardner, A. Recent mass changes of glaciers in the Russian High Arctic. *Geophys. Res. Lett.* **2012**, *39*, 1–5. [CrossRef]
41. Grant, K.; Stokes, C.; Evans, I. Identification and characteristics of surge-type glaciers on Novaya Zemlya, Russian Arctic. *J. Glaciol.* **2009**, *55*, 194. [CrossRef]
42. Zeeberg, J. *Climate and Glacial History of the Novaya Zemlya Archipelago, Russian Arctic*; Rozenberg Publishers: Amsterdam, The Netherlands, 2001.
43. Dowdeswell, J. Glaciers in the High Arctic and recent environmental change. *Philos. Trans. Phys. Sci. Eng.* **1995**, *352*, 321–334. [CrossRef]
44. Barr, S. *Franz Josef Land*; Norwegian Polar Institute: Oslo, Norway, 1995, ISBN 82-7666-095-9.
45. DLR EOC—Earth Observation Center. *TanDEM-X Ground Segment DEM Products Specification Document*; Issue 3.0; German Aerospace Center (DLR): Cologne, German, 2013.
46. Mohr, J.J.; Reeh, N.; Madsen, S. Three-dimensional glacial flow and surface elevation measured with radar interferometry. *Nature* **1998**, *391*, 273–276. [CrossRef]
47. Murray, T.; Strozzi, T.; Luckman, A.; Jiskoot, H.; Christakos, P. Is there a single surge mechanism? Contrasts in dynamics between glacier surges in Svalbard and other regions. *J. Geophys. Res.* **2003**, *108*, 2237. [CrossRef]

48. Rignot, E.; Echelmeyer, K.; Krabill, W. Penetration depth of interferometric synthetic-aperture radar signals in snow and ice. *Geophys. Res. Lett.* **2001**, *28*, 3501–3504. [CrossRef]
49. Paul, P.; Bolch, T.; Briggs, K.; Kääb, A.; McMillan, M.; McNabb, R.; Nagler, T.; Nuth, C.; Rastner, P.; Strozzi, T.; et al. Error sources and guidelines for quality assessment of glacier area, elevation change, and velocity products derived from satellite data. *Remote Sens. Environ.* **2017**, in review.
50. Voytenko, D. Glaciological Applications of Terrestrial Radar Interferometry. Ph.D. Thesis, University of South Florida, Tampa Bay, FL, USA, 2015.